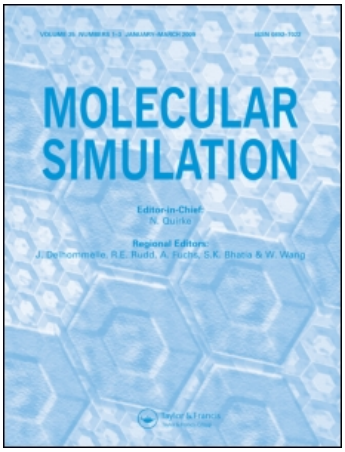

Molecular Simulation
Publication details, including instructions for authors and subscription information:
http://www.informaworld.com/smpp/title~content=t713644482

Nonadditive Monte Carlo Simulation of Liquid Hydrogen Chloride Difference Algorithm and Parallel Implementation

O. Steinhauser[a]; S. Boresch[a]; H. Bertagnolli[b]
[a] Institut für Theoretische Chemie, Universität Wien, Vienna, Austria [b] Institut für Physikalische Chemie, Universität Würzburg, Würzburg, Germany

To cite this Article Steinhauser, O. , Boresch, S. and Bertagnolli, H.(1991) 'Nonadditive Monte Carlo Simulation of Liquid Hydrogen Chloride Difference Algorithm and Parallel Implementation', Molecular Simulation, 7: 1, 71 — 88
To link to this Article: DOI: 10.1080/08927029108022449
URL: http://dx.doi.org/10.1080/08927029108022449

Molecular Simulation, 1991, Vol. 7, pp. 71–88
Reprints available directly from the publisher
Photocopying permitted by license only

NONADDITIVE MONTE CARLO SIMULATION OF LIQUID HYDROGEN CHLORIDE DIFFERENCE ALGORITHM AND PARALLEL IMPLEMENTATION

O. STEINHAUSER and S. BORESCH

Institut für Theoretische Chemie, Universität Wien, Währingerstraße 17, A-1090 Vienna, Austria

H. BERTAGNOLLI

Institut für Physikalische Chemie, Universität Würzburg, Marcusstraße 9-11, D-W-8700 Würzburg, Germany

(*Received April 1990, accepted October 1990*)

This paper continues our Monte Carlo simulation study of liquid hydrogen chloride [1]. The importance of non-additive interactions is carefully analyzed. Computed atom pair correlation functions are compared to neutron scattering experiments [2]. A difference algorithm ("Δ – algorithm") is developed, which makes non-additive Monte Carlo simulations practicable. We also report an implementation of this algorithm on a transputer network, taking advantage of the inherent parallelism of the Δ – algorithm.

KEY WORDS: Liquid hydrogen chloride, non-additive interactions, difference algorithm, transputer network.

1. INTRODUCTION

A system currently being investigated in our department is liquid hydrogen chloride. Our simulation stands in the tradition of quite a number of Monte Carlo (MC) and/or Molecular Dynamics (MD) studies [3–10]. Just recently, density dependent structure factors of liquid DCl have become available [2]. In a previous paper [1], we derived a new HCl intermolecular potential, which already includes non-additive polarization forces. This non-additive potential was already tested in MC simulations. Due to the high computational effort, however, the number of particles was restricted to $N = 64$. In this paper we shall develop an algorithm which allows non-additive MC simulations for larger particle numbers ($N = 256$) in reasonable time.

In calculating non-additive polarization forces, the central quantity is the induced dipole moment $\vec{\mu}_i$, which is obtained by solving the system of linear equations

$$\vec{\mu}_i = \alpha \cdot \left\{ \vec{E}_{i,o} + \sum_{j=1}^{N} \vec{T}_{ij} \cdot \vec{\mu}_j \cdot (1 - \delta_{ij}) \right\} \tag{1.1}$$

by a self-consistent iteration procedure (to which we shall refer as SCF – cycle). Equation (1.1) is formulated in the traditional approach, using absolute quantities. However, it is inherent to any MC scheme that it operates with differences between two successive steps and not with the absolute values. Our difference algorithm

(= Δ-algorithm) reformulates equation (1.1) in terms of the increment in induced dipole moments $\Delta\vec{\mu}_i = \vec{\mu}_i^{new} - \vec{\mu}_i^{old}$.

As shown in more detail in section 4, the Δ-algorithm reduces the number of elements entering equation (1.1). The remaining summation can be performed efficiently by exploiting the capabilities of a parallel computer. As a transputer network is available in our department, we had parallelization in mind from the very beginning.

In the following chapter, some technical aspects concerning the hard- and software of our transputer network are briefly summarized. In chapter 3 details of the HCl intermolecular potential are given. A thorough derivation of the Δ-algorithm is presented in chapter 4 together with some details of the parallel implementation. Finally, chapter 5 and 6 deal with the actual MC simulations and the results thereby obtained.

2 TECHNICAL ASPECTS OF HARD AND SOFTWARE

2.1 *System description*

Several parallel computer systems are commercially available. For our problems, however, a transputer based system offers the best price vs. performance relation. A transputer is a single chip containing the processor, (a small amount of) memory and communication links which provide synchronized point to point connection between transputers. Using these devices a network of transputers is easily constructed [11].

The six-membered ring shown in figure 1 is our pilot system, which consists of three components:

a) The host computer is an IBM-AT

b) The AT houses a Microway transputer board (Master equipped with a 20 MHz Inmos T800 and 4 Megabytes of RAM.) These two hardware components communicate via the PC-bus and the C012 link adaptor using the software file

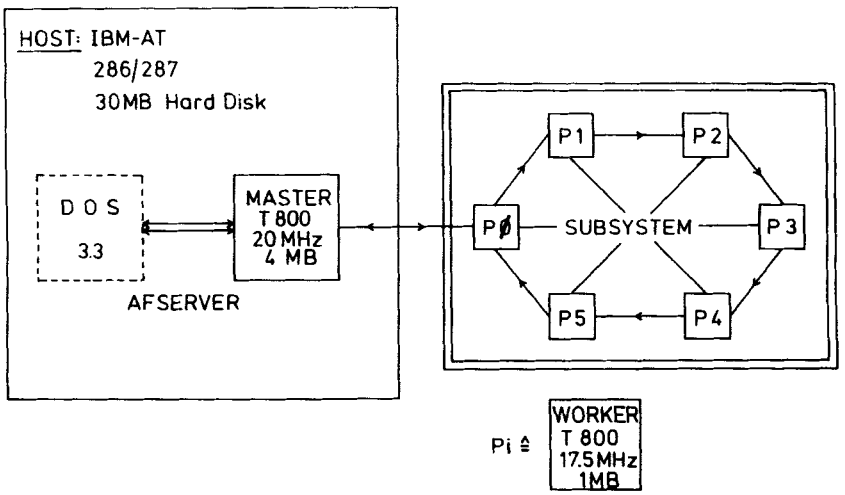

Figure 1 Small pilot system: configuration of host computer and transputer network.

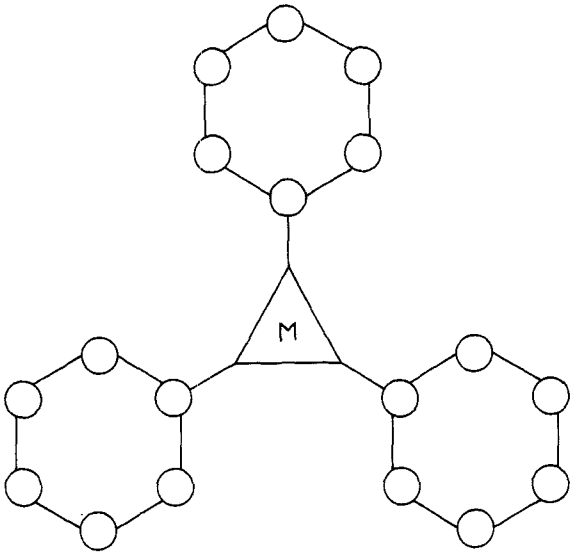

Figure 2 "Clover-leaf" structure of the large transputer subsystem.

server protocol "afserver.exe" contained in the compiler package. Thus the master transputer can access the hard disk and I/O devices of the host.

c) Numerically intensive parts of a program run on the subsystem, which was assembled by an Austrian company, IMPULS Computer Systems. This subsystem consists of six boards, each carrying a 17.5 MHz T800 transputer and 1MB of RAM. Communication between master and subsystem (P0) and in the subsystem itself proceeds via the transputer-links in a bus-less manner.

Based on the experience with this pilot system, we have acquired an 18 processor system, which consists of three replica of the subsystem described. This "clover-leaf structure" is shown in Figure 2. Most of the MC simulations reported here were performed on this extended transputer network.

The new system accelerates our non-additive MC simulations by a factor of 2.5 as compared to the pilot system. This comes close to the theoretical factor of 3. Altogether, the computational power of the larger system rivals that of an IBM 3090 mainframe in scalar mode.

2.2 *Compiler Features*

Since 1988 a parallel FORTRAN compiler for transputer systems has been available [12]. This compiler manages communication by calling dedicated subroutines from a runtime library.

2.2.1 *Runtime Library*

We always run only one program (a task) on each processor. Therefore, we need a single package ('CHAN.INC') out of the various options of the runtime library. From

this package itself, we use only the simple communication routines

F77_CHAN_IN_MESSAGE (LENGTH, FIELD, INADDR) (2.1)

for receiving and

F77_CHAN_OUT_MESSAGE (LENGTH, FIELD, IOUTADDR) (2.2)

for sending. Here LENGTH is the number of bytes of array FIELD to be sent, and INADDR/IOUTADDR is the address of the respective hardware channel given as a constant in the 'CHAN. INC' package.

If only a 4 byte word (e.g. INTEGER, REAL*4) has to be sent, (2.1) and (2.2) simplify to

F77_CHAN_IN_WORD (VARIABLE, INADDR) (2.3)

F77_CHAN_OUT_WORD (VARIABLE, IOUTADDR) (2.4)

2.2.2 *The Configurer*

All tasks to be loaded on the processors have to be compiled and linked separately. From these component tasks a bootable application image file has to be generated. This is performed by the configurer, which is driven by a so called configuration file specifying

a) the hardware configuration,
b) the names of the component tasks,
c) the placement of particular tasks onto particular processors in the physical network.

The output of the configurer is a bootable program which can be loaded into the network using the 'afserver.exe' (the server program running on the DOS–host). A typical example from our application is given in the appendix.

3. CHEMICAL MODEL

The intermolecular potential between a pair of molecules i and j is given by

$$U_{ij} = U_{LJ} + U_{EL} + U_{POL} \tag{3.1}$$

It is modelled by a two center Lennard Jones potential,

$$U_{LJ} = \sum_{A=1}^{2} \sum_{B=1}^{2} 4\varepsilon_{AB} \cdot \left\{ \left(\frac{\sigma_{AB}}{r_{AB}} \right)^{12} - \left(\frac{\sigma_{AB}}{r_{AB}} \right)^{6} \right\} \tag{3.2}$$

a six center Coulomb interaction,

$$U_{EL} = \sum_{A=1}^{6} \sum_{B=1}^{6} \frac{q_A \cdot q_B}{r_{AB}} \tag{3.3}$$

and the non-additive polarization contribution explained in detail in chapter 4.

The procedure of obtaining the respective potential parameters from *ab initio* data [13] has been fully described in our previous publication [1]. Therefore, we give only

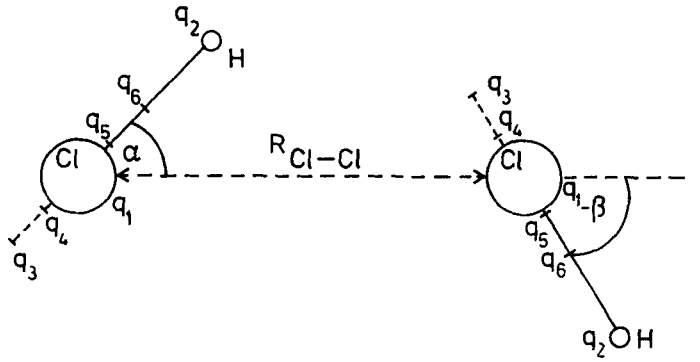

Figure 3 Geometric arrangement of a HCl dimer. The charge distribution of the molecule is described by six point charges, positioned along the molecular axis at $\pm 0.25\, r_{HCl}$ (q_4, q_5), at $\pm 0.50\, r_{HCl}$ (q_3, q_6), at r_{HCl} (q_2) and at the Cl atom (q_1).

the results here:

$$\varepsilon_{HCl} = 0.70\,\text{kJ/mol} \qquad \sigma_{HCl} = 0.24\,\text{nm}$$
$$\varepsilon_{ClCl} = 1.25\,\text{kJ/mol} \qquad \sigma_{ClCl} = 0.37\,\text{nm} \tag{3.4}$$

As *ab initio* calculations had shown that hydrogen–hydrogen interactions had little influence on the dimer properties, they were omitted, i.e. $\varepsilon_{HH} = 0.0\,\text{kJ/mol}$.

The set of charges

$$\begin{aligned} q_1 &= q_{Cl} = -1.38\,e \\ q_2 &= q_H = +0.18\,e \\ q_3 &= -0.13\,e \\ q_4 &= +1.46\,e \\ q_5 &= -1.46\,e \\ q_6 &= +1.33\,e \end{aligned} \tag{3.5}$$

results from a superposition of physical multipoles representing the correct *ab initio* dipole

$$-q_1 = +q_2 = 0.18e, \tag{3.6a}$$

quadrupole

$$-q_1'/2 = q_3' = q_6' = 0.60e \tag{3.6b}$$

and octopole moment

$$-q_3'' = q_4''/2 = -q_5''/2 = q_6'' = 0.73e. \tag{3.6c}$$

Site 1 and 2 correspond to the position of the chlorine and hydrogen atom. Sites 3 to 6 are located at -0.50, -0.25, $+0.25$ and $+0.50\, \vec{r}_{HCl}$. This spatial arrangement of charges is also shown graphically in Figure 3.

The molecular polarizability α is the only quantity necessary for the calculation of the nonadditive part of the potential:

$$\alpha = 2.53 \cdot 10^{-3}\,\text{nm}^3 \tag{3.7}$$

4. TECHNIQUE OF NON-ADDITIVE MONTE CARLO

The mathematical treatment of polarization forces depends whether the permanent charge distribution is modelled by mathematical multipoles or point charges. The first approach is somewhat more common [14] whereas there are only few examples in the literature using point charges [15–17]. Due to the slow convergence properties of the mathematical multipole series, we use the six center point charge model summarized in equation (3.5).

4.1 *Non-additive Polarization Forces*

The contribution of the polarization to the total potential energy is given by

$$U_{\mathrm{POL}} = -\sum_{i=1}^{N} \vec{\mu}_i \cdot \vec{E}_{i,\mathrm{o}} - \frac{1}{2}\sum_{i=1}^{N}\sum_{j=1}^{N} \vec{\mu}_i \cdot \vec{T}_{ij} \cdot \vec{\mu}_j (1 - \delta_{ij}) + \frac{1}{2}\sum_{i=1}^{N} \vec{\mu}_i^2/\alpha \qquad (4.1)$$

where

$$\vec{E}_{i,\mathrm{o}} = \sum_{j=1}^{N}\sum_{B=1}^{6} \frac{q_B \cdot (\vec{r}_i - \vec{r}_{jB})}{|\vec{r}_i - \vec{r}_{jB}|^3} \cdot (1 - \delta_{ij}) \qquad (4.2)$$

is the electric field exerted by all permanent charges q_B on chlorine atom i. The corresponding field generated by all induced dipoles $\vec{\mu}_j$ is given by

$$\vec{E}_{i,\mathrm{ind}} = \sum_{j=1}^{N} \vec{T}_{ij} \cdot \vec{\mu}_j \cdot (1 - \delta_{ij}) \qquad (4.3)$$

with

$$\vec{T}_{ij} = r_{ij}^{-3} \cdot \left\{ 3\,\frac{\vec{r}_{ij} : \vec{r}_{ij}}{r_{ij}^2} - \delta_{ij} \right\} \qquad (4.4)$$

being the well known dipole tensor. $\vec{r}_{ij}$ is the vector joining chlorine atoms i and j. The last term in equation (4.1) is the so-called self-energy containing the molecular polarizability α.

For every Monte Carlo move, U_{POL} has to be minimized, i.e.

$$\frac{\partial U_{\mathrm{POL}}}{\partial \vec{\mu}_i} = 0 \qquad \text{for all } i \qquad (4.5)$$

which leads to the equivalent expression (1.1). If relation (1.1) is substituted into (4.1), the second and third term vanish, and only one half of the first term is left.

$$U_{\mathrm{POL}}^{\mathrm{min}} = -\frac{1}{2}\sum_{i=1}^{N} \vec{\mu}_i \cdot \vec{E}_{i,\mathrm{o}} \qquad (4.6)$$

It should be noted that (4.6) is just the minimum of the general expression (4.1). In principle the system of linear equations (1.1) for the induced moments may be solved by matrix inversion. A more efficient way, however, is provided by an iterative solution algorithm, i.e. a *S*elf-*C*onsisting-*F*ield-cycle.

4.2 *"Group-move" concept*

Before developing the Δ-algorithm, one has to realize that moving a particle has utterly different consequences in additive and nonadditive MC: According to equation (1.1), moving a single particle already changes the complete set of induced dipole

moments, thus requiring a new SCF-cycle. It therefore is more efficient to move a group of NSEL randomly selected particles simultaneously. This means, however, that all quantities appearing in the MC scheme, i.e.

the additive enery contribution $U_{ij}^{\text{add}} = U_{LJ} + U_{EI}$

the permanent field $\vec{E}_{i,o}$

and the dipole–dipole tensor $\vec{T}_{ij}$,

have to be adapted to this group move concept. Fortunately, all these quantities have a common feature: Either they are a pair matrix themselves, like $\vec{T}_{ij}$, or they result from a summation over pair matrix elements (U^{add}, $\vec{E}_{i,o}$). If particle indices (= array indices) are reordered in such a way that

(1) particles selected for moving have indices 1:NSEL,

(2) the particles to remain unchanged in this particular MC step have indices NSEL + 1:N and

(3) the array indices are not changed in any further respect,

the matrix of pair interactions displays the structure shown in Figure 4. The shaded area represents those entries which are really changed between two successive steps. If NSEL particles are selected out of N particles, the strip shown in Figure 4 has dimensions

$$(\text{NSEL*N}) - \frac{\text{NSEL*(NSEL + 1)}}{2}. \tag{4.7}$$

The second term represents the lower triangle and follows from the exchange symmetry

$$\vec{A}_{ji} = \pm \vec{A}_{ij} \tag{4.8}$$

for all quantities mentioned above.

4.3 Δ-*Algorithm*

As already pointed out in the introduction, it is not the absolute value of the polarization energy (4.6) that enters the MC scheme, but the difference in the polarization energy between two successive steps:

$$\Delta U_{\text{Pol}} = U_{\text{Pol}}^{\text{New}} - U_{\text{Pol}}^{\text{Old}} \tag{4.9}$$

Denoting the increment in the induced moment by $\Delta\vec{\mu}_i$ and the increment in the permanent field by $\Delta\vec{E}_{i,o}$, equation (4.6) takes the explicit form

$$\Delta U_{\text{Pol}} = -\frac{1}{2}\sum_{i=1}^{N}\left[(\vec{\mu}_i + \Delta\vec{\mu}_i)(\vec{E}_{i,o} + \Delta\vec{E}_{i,o}) - (\vec{\mu}_i\vec{E}_{i,o})\right] \tag{4.10}$$

$$\Delta U_{\text{Pol}} = -\frac{1}{2}\left(\Delta U_{\text{Pol}}^{(1)} + \Delta U_{\text{Pol}}^{(2)}\right)$$

$$\Delta U_{\text{Pol}}^{(1)} = \sum_{i=1}^{N}\vec{\mu}_i\Delta\vec{E}_{i,o}$$

$$\Delta U_{\text{Pol}}^{(2)} = \sum_{i=1}^{N}\Delta\vec{\mu}_i\left(\vec{E}_{i,o} + \Delta\vec{E}_{i,o}\right) \tag{4.11}$$

$\Delta U_{\mathrm{Pol}}^{(1)}$ doesn't require the SCF iteration cycle as it contains the induced moments $\vec{\mu}_j$ of the previous step and the increment of the permanent field. For the evaluation of $\Delta U_{\mathrm{Pol}}^{(2)}$ we need the increments of the induced dipole moments $\Delta\vec{\mu}_i$.

If one applies the idea of a Δ-algorithm not only to the energy U_{Pol} but to all other quantities $\vec{\mu}_i$, $\vec{E}_{i,\mathrm{o}}$, $\vec{T}_{ij}$, entering equation (1.1), one obtains:

$$\Delta\vec{\mu}_i = \alpha \left\{ \Delta\vec{E}_{i,\mathrm{o}} + \sum \Delta\vec{T}_{ij}\vec{\mu}_j(1 - \delta_{ij}) \right. \tag{4.12a}$$

$$+ \sum \Delta\vec{T}_{ij} \cdot \Delta\vec{\mu}_j \cdot (1 - \delta_{ij}) \tag{4.12b}$$

$$\left. + \sum_{j=1}^{N} \vec{T}_{ij} \cdot \Delta\vec{\mu}_j \cdot (1 - \delta_{ij}) \right\} \tag{4.12c}$$

This formal reorganization of equation (1.1) shows its merits only in connection with the group move concept. The "Δ-quantities" $\Delta\vec{E}_{i,\mathrm{o}}$ and $\Delta\vec{T}_{ij}$ originate from those pair matrix elements where at least one particle has been moved. In other words, only the shaded area of Figure 4 has to be recalculated, which represents a small number of pair elements (4.7) compared to the complete matrix containing N·(N–1)/2 elements.

As far as the SCF-cycle is concerned, the two terms of equation (4.12a) are a constant and serve as a starting value. The summation in (4.12b) is drastically reduced because it refers to the "Δ-quantity" $\Delta\vec{T}_{ij}$. A summation over the whole pair matrix has to be done for the last term (4.12c) only. Thus (4.12c) is *the* time consuming part of the iteration cycle. If the updating procedure given below is done properly, the dipole dipole tensor $\vec{T}_{ij}$ of the previous step may be used without any additional recalculation.

The SCF-cycle delivers the missing contribution $\Delta U_{\mathrm{Pol}}^{(2)}$ to the energy difference between two successive MC steps. If the configuration is rejected, a new MC step begins. In case of acceptance $\vec{T}_{ij}$, $\vec{E}_{i,\mathrm{o}}$ and $\vec{\mu}_i$ have to be updated with their respective increments $\Delta\vec{T}_{ij}$, $\Delta\vec{E}_{i,\mathrm{o}}$ and $\Delta\vec{\mu}_i$.

4.4 *Parallel implementation*

4.4.1 *Initialization*

Before starting the actual MC runs, all processors of the subsystem receive necessary control parameters and constants, like processor number and potential parameters, as well as the complete set of coordinates. In this initializing step the master also calculates the permanent field $\vec{E}_{i,\mathrm{o}}$ and the T-Tensor $\vec{T}_{ij}$, which serve as starting values for the Δ-algorithm. The T-Tensor $\vec{T}_{ij}$ is sent to the subsystem. Furthermore, the master generates masks, which the subsystem needs for loadbalancing.

4.4.2 *Additive contributions including permanent field*

Loadbalancing is achieved by distributing the shaded area of Figure 4 among all processors. The upper triangle and a suitable part of the rectangular strip are calculated by the master, and the remaining work is handled by the subsystem.

In each MC step the coordinates of the group selected for the next move are generated by the master and are submitted to the subsystem. Each processor evaluates ΔU^{add} and $\Delta\vec{E}_{i,\mathrm{o}}$ for its partition; the partial results are accumulated and sent to the master.

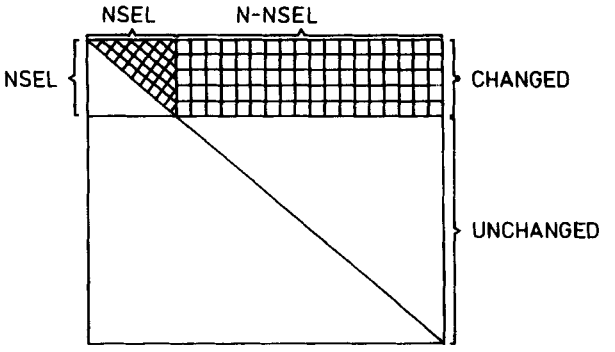

Figure 4 Graphical representation of the pair matrix in the group move concept. Only the shaded area is changed. After a suitable reordering of particle indices described in the text, changes appearing in a particular MC step are confined to the shaded area.

4.4.3 *SCF-cycle*

The iteration cycle affects the terms (4.12b) and (4.12c). As already discussed in section (4.3), equation (4.12c) represents the most time consuming part. Therefore, (4.12b) is evaluated on the master as parallelization would not be rewarding. (4.12c), referencing the complete T-Tensor, is calculated by the subsystem using the following mapping technique.

The strategy we have chosen is best described by the graphical representation given in Figure 5. If the complete pair matrix is divided in n partitions and the general symmetry relation (4.8) holds, we have $(n \cdot (n - 1)/2)$ offdiagonal blocks. If n is even, the diagonal triangles can be pairwise united to form $(n/2)$ complete blocks. Altogether we have $(n \cdot (n - 1)/2) + (n/2) = (n^2/2)$ blocks that have to mapped on m transputers:

$$\frac{n^2}{2} = f \cdot m \tag{4.13}$$

f is the number of blocks assigned to a single transputer. For our pilot system, m is six and n is six which leads to $f = 3$ as indicated in Figure 5. In the case of 18 processors $f = 1$.

The necessity for a correct updating procedure has already been pointed out. In a parallel implementation of the Δ-algorithm, $\vec{T}_{ij}$, $\vec{E}_{i,o}$ and $\vec{\mu}_i$ have to be updated on each processor, provided the move was accepted.

5. DETAILS OF THE MONTE CARLO RUNS

The number of particles was $N = 256$. Molecules were confined to a cubic box, and toroidal boundary conditions were applied. For all MC runs pair interactions exceeding a spatial threshold $r_c > 1.05$ nm were truncated. The two densities $\rho = 13.8\,\text{nm}^{-3}$ and $\rho = 8.1\,\text{nm}^{-3}$ correlate to a box length of 2.65 and 3.16 nm respectively. Simulations were performed at 25°C and 100°C. The starting configurations were those obtained from the additive simulations already published [1].

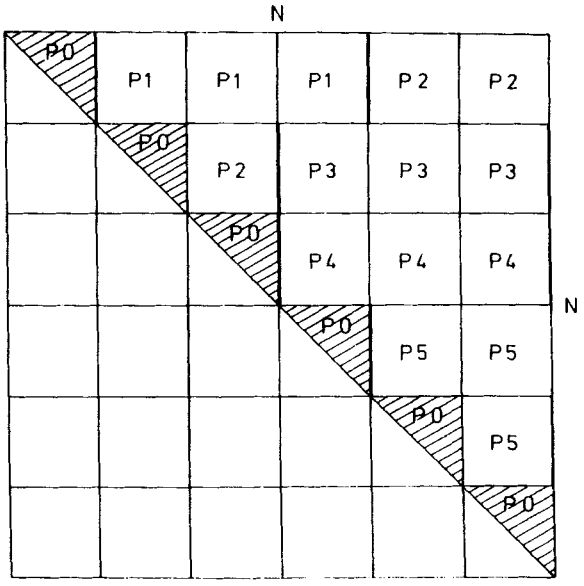

Figure 5 Outline of the block structure algorithm and assignment of blocks to specific processors for our transputer network.

Further details of these four MC runs are summarized in Tables 1 and 2. We are aware that the lower density represents a hypothetical state, which is experimentally not accessible. It was merely included for completeness sake.

As we performed group moves with NSEL = 8 particles (section 4.3), the translational and rotational step sizes were by an order of magnitude smaller compared to single particle moves in order to keep the rate of acceptance high enough. Chlorine atoms were randomly shifted by a maximum amount of ± 0.02 nm. Molecular orientation was changed by random rotation about a suitably chosen unit vector, the direction cosines of which were also random numbers. The maximum angle of rotation was $\pm 2°$.

Table 1 Simulation average energies and other details of the MC runs (room temperature). R_{max} is the cutoff-radius.

MC	$\rho = 8.1\,nm^{-3}$	$\rho = 13.8\,nm^{-3}$
Box length c/nm	3.16	2.65
Number of particles	256	256
R_{max}/nm	1.05	1.05
Temperature/C	25	25
Translational [nm] and	0.02	0.02
rotational displacement	2°	2°
8 particle moves	640000	544000
Acceptance in %	66	57
U/kJ·mol^{-1}	−7.55	−10.56
U_{LJ}/kJ·mol^{-1}	−3.86	−5.76
U_{EI}/kJ·mol^{-1}	−2.93	−3.82
U_{Pol}/kJ·mol^{-1}	−0.76	−0.98

Table 2 Simulation average energies and other details of the MC runs (supercritical fluid). R_{max} is the cutoff-radius.

MC	$\rho = 8.1\,nm^{-3}$	$\rho = 13.8\,nm^{-3}$
Box length c/nm	3.16	2.65
Number of particles	256	256
R_{max}/nm	1.05	1.05
Temperature/C	100	100
Translational [nm] and	0.02	0.02
rotational displacement	2°	2°
8 particle moves	480000	480000
Acceptance in %	71	61
U/kJ·mol^{-1}	−6.55	−9.81
U_{LJ}/kJ·mol^{-1}	−3.59	−5.55
U_{El}/kJ·mol^{-1}	−2.31	−3.34
U_{Pol}/kJ·mol^{-1}	−0.66	−0.92

6. RESULTS AND DISCUSSION

6.1 *Effects of density variation in simulation*

6.1.1 *Room temperature (25°C)*

Figure 6 compares pair correlation functions for the two densities $\rho = 13.8\,nm^{-3}$ (solid line) and $\rho = 8.1\,nm^{-3}$ (dashed line). Figure 6a contains the Cl–Cl, Figure 6b H–Cl and H–H correlation functions.

Neutron scattering experiments yield the weighted superposition of the individual atom pair correlation functions [2]

$$G(r) = 0.384\, g_{ClCl}(r) + 0.484\, g_{HCl}(r) + 0.168\, g_{HH}(r) \qquad (6.1)$$

The equation is formulated for deuterium chloride as diffraction experiments were performed with this substance. $G(r)$ – as obtained from simulation – is shown in Figure 6c.

The influence of density is clearly visible: Although in all correlation functions the positions of maxima and minima are unaltered, their absolute height is affected. The height of the respective first maxima is generally higher at the lower density. This effect shows up significantly in g_{HCl} and g_{HH}, whereas it is small in g_{ClCl}. Especially the first maximum of the hydrogen chlorine correlation function is more pronounced at the lower density. This is discernible even in the weighted superposition (see Figure 6c). On the other hand, at distances $r > 0.4$ nm, especially for the chlorine – chlorine correlation, oscillations around the reference line 1.0 are stronger at the higher density. They indicate correlations to subsequent neighbours and are almost completely missing at the lower density.

6.1.2 *Supercritical fluid (100°C)*

Figure 7 is the high temperature counterpart of Figure 6. All correlation functions are somewhat blurred as compared to the lower temperature (25°C). Nevertheless, the effect of density variation is still visible and is similar to that observed at room temperature: The respective first maxima in the individual pair correlation functions are higher at the lower density, whereas stronger correlations to subsequent neighbors exist at the higher density.

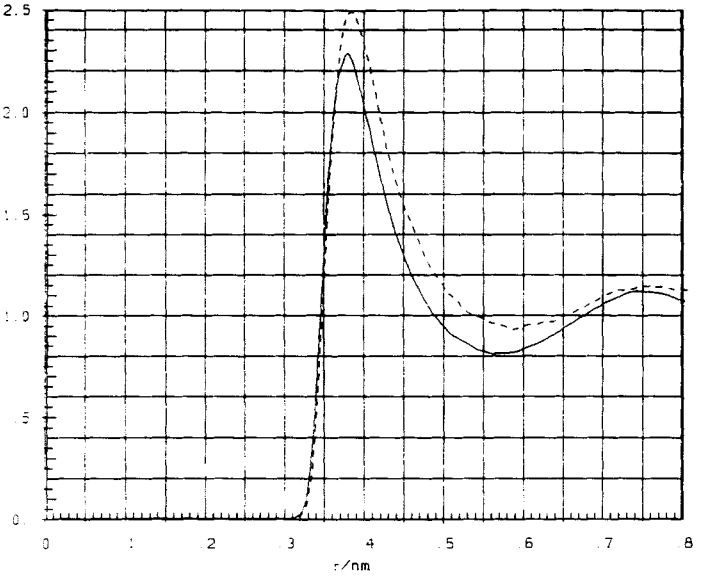

Figure 6a Chlorine–Chlorine pair correlain functions $g_{ClCl}(r)$ at 25°C for densities $\rho = 13.8\,\mathrm{nm}^{-3}$ (solid line) and $\rho = 8.1\,\mathrm{nm}^{-3}$ (dashed line).

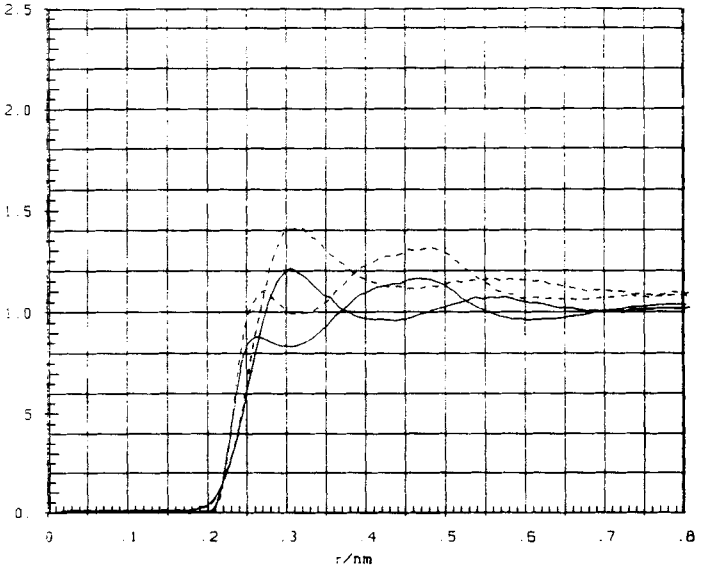

Figure 6b Hydrogen–Hydrogen $g_{HH}(r)$ and Hydrogen–Chlorine $g_{HCl}(r)$ pair correlation functions at 25°C for densities $\rho = 13.8\,\mathrm{nm}^{-3}$ (solid line) and $\rho = 8.1\,\mathrm{n},^{-3}$ (dashed line). g_{HH} and g_{HCl} may be distinguished by the height of the respective first maximum, which is higher for g_{HH}.

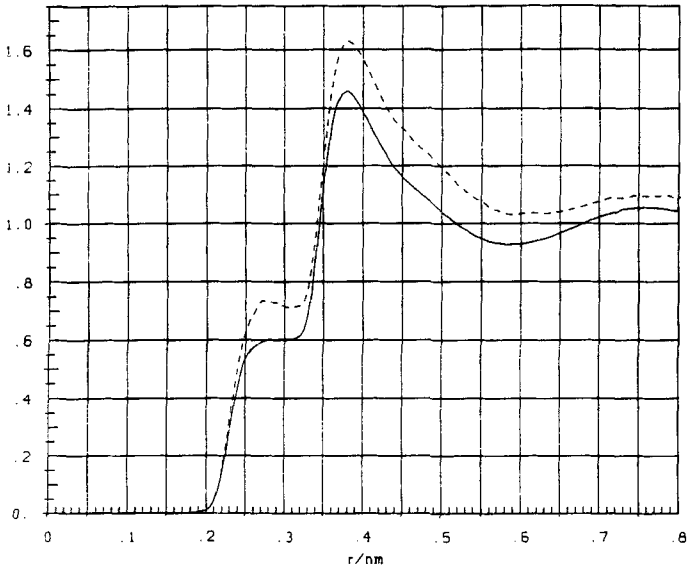

Figure 6c Simulated weighted superposition of atom pair correlation functions (cf. eqn. 6.1) at $T = 25°C$ for densities $\rho = 13.8\,nm^{-3}$ (solid line) and $\rho = 8.1\,nm^{-3}$ (dashed line).

6.2 *Effects of density variation in experiment*

The experimental $G(r)$ for the two densities $\rho = 13.8\,nm^{-3}$ (solid line) and $\rho = 8.1\,nm^{-3}$ (dashed line) at 100°C are presented in Figure 8. At the lower density the first maximum (at $r = 0.27$ nm) becomes more distinct; furthermore, a third peak at $r = 0.45$ nm appears. Both features can be recognized in the simulation (cf. Figure 7c): The shoulder at 0.29 nm is higher at the lower density, just as the descent after the peak at 0.38 nm exceeds its counterpart at the higher density.

The experiments suggest that the dominant structural element – the dimer – is less disturbed by surrounding neighbors at the lower density. Such a behavior is reflected in the simulation: The fact that the absolute height of the respective first maximum is larger at the lower density – and this found in all individual pair correlation functions – is a clear indication.

6.3 *Comparison of experiment and simulation*

Figure 9 compares the experimental result (dashed line) with simulated $g(r)$ (solid line) for $\rho = 13.8\,nm^{-3}$ at $T = 25°C$. The general features of the experiment are described quite well; especially for distances $r > 0.45$ nm the agreement is excellent. There are two main differences between simulation and experiment: The distinct first maximum of the experiment ($r = 0.27$ nm) degenerates to a very flat one or even to a shoulder at $r = 0.29$ nm in simulation. Furthermore, in the MC calculations the dominant second peak is constantly shifted to slightly smaller intermolecular distances ($\cong 0.38$ nm compared to the experimental 0.40 nm). Both findings are also observed for the two states at 100°C.

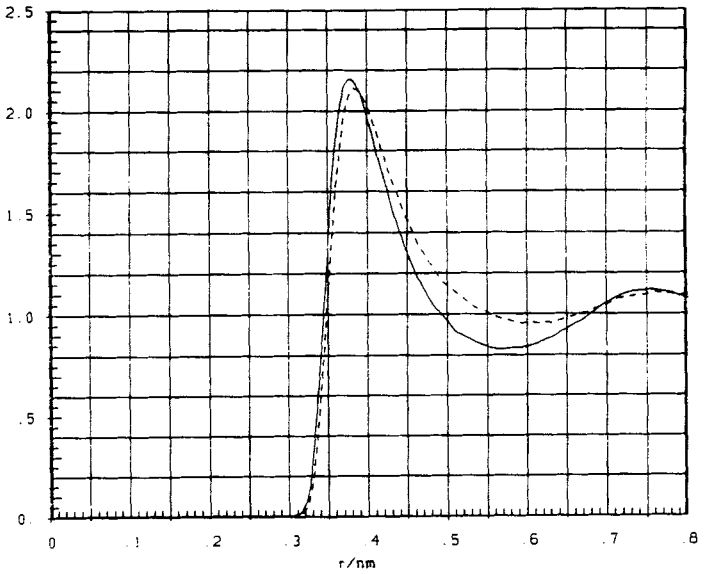

Figure 7a Chlorine–Chlorine pair correlation functions $g_{ClCl}(r)$ at 100°C for densities $\rho = 13.8\,\mathrm{nm}^{-3}$ (solid line) and $\rho = 8.1\,\mathrm{nm}^{-3}$ (dashed line).

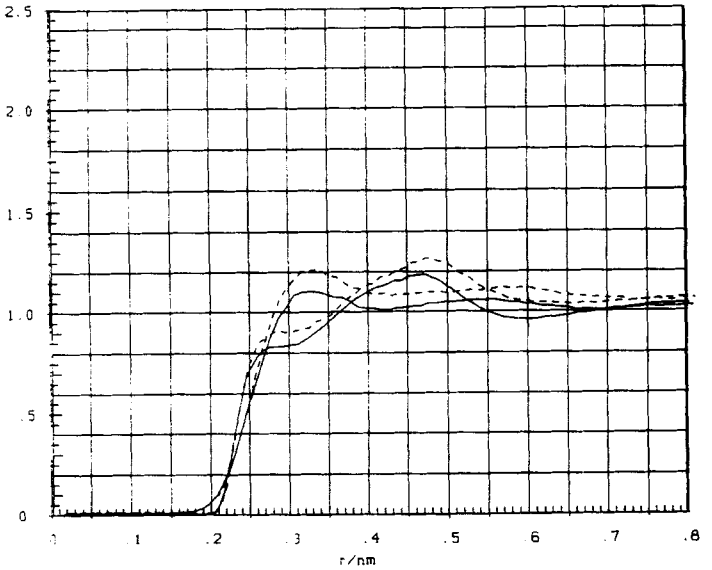

Figure 7b Hydrogen–Hydrogen $g_{HH}(r)$ and Hydrogen–Chlorine $g_{HCl}(r)$ pair correlation functions at 100°C for densities $\rho = 13.8\,\mathrm{nm}^{-3}$ (solid line) and $\rho = 8.1\,\mathrm{nm}^{-3}$ (dashed line). g_{HH} and g_{HCl} may be distinguished by the height of the respective first maximum, which is higher for g_{HH}.

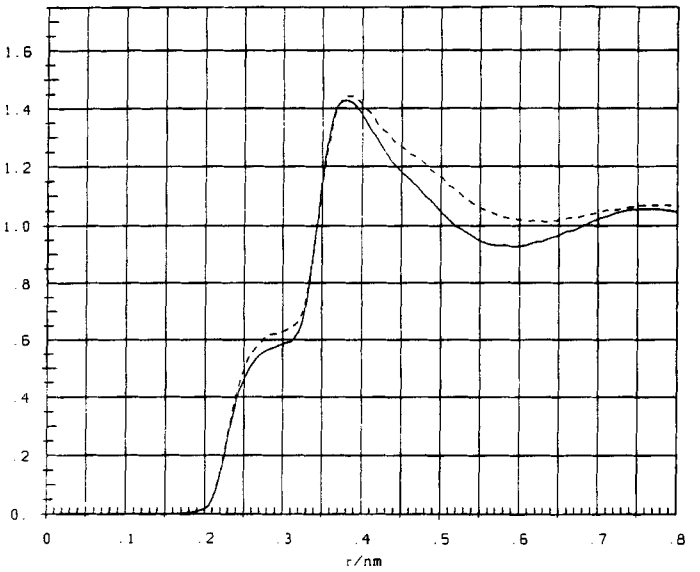

Figure 7c Simulated weighted superposition of atom pair correlation functions (cf. eqn. 6.1) at $T = 100°C$ for densities $\rho = 13.8\,nm^{-3}$ (solid line) and $\rho = 8.1\,nm^{-3}$ (dashed line).

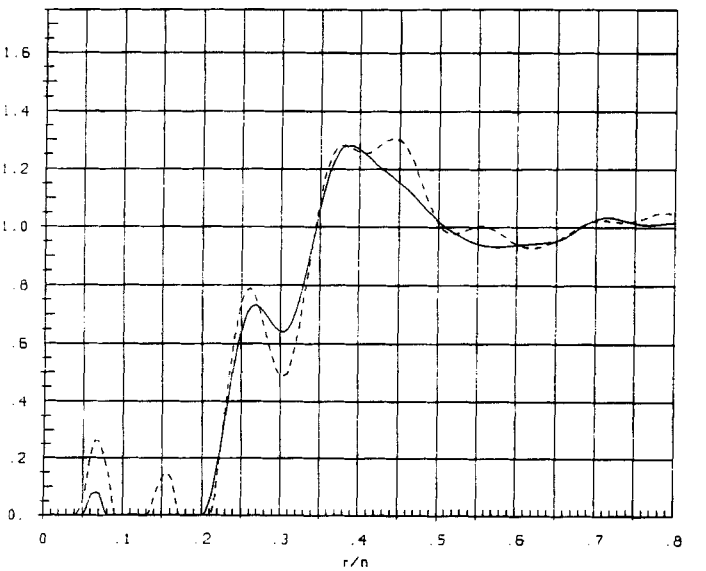

Figure 8 Comparison of Fourier transformed neutron diffraction data (threshold for Fourier transformation was $8.0\,nm^{-1}$) for densities $\rho = 13.8\,nm^{-3}$ (solid line) and $\rho = 8.1\,nm^{-3}$ (dashed line) at $T = 100°C$.

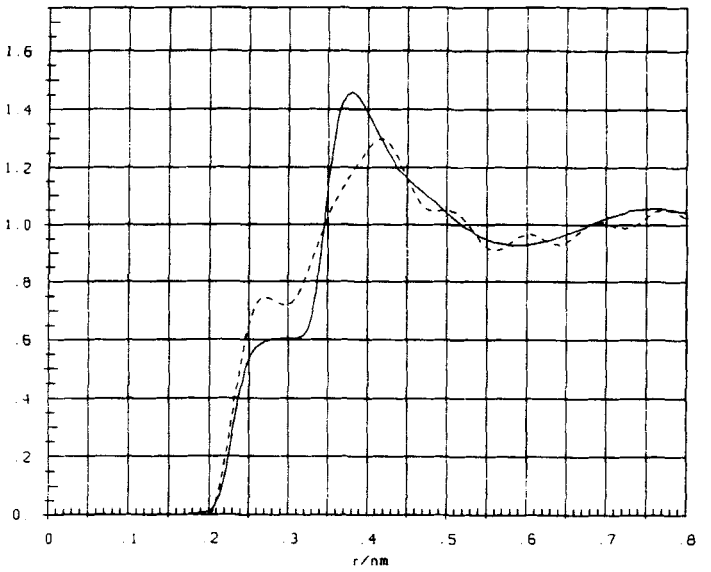

Figure 9 Weighted superposition (see equation (6.1)) of atom pair correlation functions at $\rho = 13.8\,\mathrm{nm}^{-3}$ and $T = 25°C$. The solid line represents non-additive MC simulation, the dashed line stands for the neutron scattering experiment [2].

The difference between experiment and simulation in the region of the first maximum at $r = 0.27\,\mathrm{nm}$ is not unexpected. It seems reasonable to attribute this peak to an intermolecular hydrogen bond. The potential employed, however, has no explicit term to mimic a hydrogen bond. This explains the differences in shape and height between simulation and experiment.

7. CONCLUSION

Obviously, non-additive MC simulations are expensive with respect to computer resources. We consider more efficient algorithms and parallelization to be the only means to overcome computational limitations. The Δ-algorithm presented in this paper is a considerable progress in both respects. Firstly, being in accordance with the difference scheme inherent to any MC technique, it reduces numerical effort. Secondly, being designed for parallelization, the actual implementation on the transputer network was readily achieved and yielded the expected speed up.

APPENDIX

Example of a config-file:

```
!
processor host                                          ! the pc
processor master                                        ! the master-transputer-board
processor p0                                            ! the 1st worker-transputer-board
processor p1                                            ! the 2nd worker-transputer-board
processor p2                                            ! the 3rd worker-transputer-board
processor p3                                            ! the 4th worker-transputer-board
processor p4                                            ! the 5th worker-transputer-board
processor p5                                            ! the 6th worker-transputer-board
!
wire ? master [0] host [0]                              ! connects link0 of the master-
!                                                       transputer to the pc bus
wire ? master [3] p0 [3]
!                                                       hardwarelinks for the ring-
wire ? p0 [1]          p1 [0]                           ! topology
wire ? p1 [1]          p2 [0]
wire ? p2 [1]          p3 [0]
wire ? p3 [1]          p4 [0]

wire ? p4 [1]          p5 [0]
wire ? p5 [1]          p0 [0]
!                                                       diagonal links
wire ? p0 [2]          p3 [2]
wire ? p1 [2]          p4 [2]
wire ? p2 [2]          p5 [2]
!                      the system-tasks
task afserver          ins = 1          outs = 1
task filter            ins = 2          outs = 2    data = 10k
!                      the user-tasks
task po12_m            ins = 3          outs = 3
task po12_s0           ins = 3          outs = 3
task po12_s1           ins = 3          outs = 3
task po12_s2           ins = 3          outs = 3
task po12_s3           ins = 3          outs = 3
task po12_s4           ins = 3          outs = 3
task po12_s5           ins = 3          outs = 3
!
place afserver host                     ! afserver runs on the pc
!
place filter           master           ! everything else on the transputer master
place po12_m           master
!
place po12_s0 p0
place po12_s1 p1
place po12_s2 p2
place po12_s3 p3
place po12_s4 p4
place po12_s5 p5
!                      necessary software connections
connect ?              filter [0]       afserver [0]
connect ?              afserver [0]     filter [0]
connect ?              po12_m [1]       filter [1]
connect ?              filter [1]       po12_m [1]
```

Acknowledgement

The results presented in section 6 were computed on a transputer network constructed by IMPULS Computer Systems, Austria. Continuous support from this company is gratefully acknowledged. Development of the respective programs is part of the research project P7421 "Chemische Simulation auf Transputersystemen" funded by the Austrian "Fond zur Förderung wissenschaftlicher Forschung".

References

[1] O. Steinhauser, S. Boresch and H. Bertagnolli, "The effect of density variation on the structure of liquid hydrogen chloride: A Monte Carlo study", *J. Chem. Phys.* **93,** 2357 (1990).
[2] T. Bausenwein, H. Bertagnolli, K. Tödheide, and P. Chieux, submitted to *Ber. Bunsenges. Phys. Chem.*
[3] J.G. Powles, W.A.B. Evans, E. McGrath, K.E. Gubbins and S. Murad, "A computer simulation for a simple model of liquid hydrogen chloride", *Mol. Phys.* **38,** 893 (1979).
[4] J.G. Powles, E. McGrath and K.E. Gubbins, "A computer simulation for a simple model of liquid hydrogen chloride-time correlation functions", *Mol. Phys.* **40,** 179 (1980).
[5] S. Murad, K.E. Gubbins and J.G. Powles, "A molecular dynamics simulation of fluid hydrogen chloride", *Mol. Phys.* **40**, 253 (1980).
[6] S. Murad, "The structure of hydrogen chloride: Dimer, liquid, and ordered solid", *Mol. Phys.* **51**, 525 (1984).
[7] S. Murad, A. Papaioannou, J.G. Powles, "A computer simulation for model fluid hydrogen chloride", *Mol. Phys.* **56**, 431 (1985).
[8] I.A. McDonald, S.F. O'Shea, D.G. Bounds, M.L. Klein, "Structure and dynamics of associated molecular systems. III. Computer simulation of liquid hydrogen chloride", *J. Chem. Phys.* **72,** 5710 (1980).
[9] D. Levesque, J.J. Weis and D.W. Oxtoby, "A molecular dynamics simulation of rotational and vibrational relaxation in liquid HCl", *J. Chem. Phys.* **79**, 917 (1983).
[10] C. Votava, R. Ahlrichs and A. Geiger, "The HCl-HCl interaction: From quantum mechanical calculations to the properties of the liquid", *J. Chem. Phys.* **78**, 6841 (1983).
[11] INMOS Limited, ed. Transputer Reference Manual, Prentice Hall, New York, 1988.
[12] 3L Parallel Fortran Compiler 2.0, Handbook, 3L Ltd., Livingstone EH54 6AG, Scotland.
[13] a) A. Karpfen, H. Lischka, P.R. Bunker, in: Dynamics of Polyatomic Van der Waals Complexes, ed. N. Halbenstedt and K. Janda, Plenum Press 1990.
b) A. Karpfen, P.R. Bunker, P. Jensen, "An ab initio study of the hydrogen chloride dimer", *Chem. Phys.*, in press.
[14] C.G. Gray, K.E. Gubbins, Theory of Molecular Fluids, Vol. 1, Clarendon Press, Oxford (1984).
[15] B.J. Costa Cabral, J.L. Rivail and B. Bigot, "A Monte Carlo study of a polarizable liquid", *J. Chem. Phys.* **86**, 1467 (1987).
[16] P. Ahlström, A. Wallquist, S. Engström, B. Jönsson, "A molecular dynamics study of polarizable water", *Mol. Phys.* **68**, 563 (1989).
[17] T.P. Straatsma, J.A. McCammon, "Free energy thermodynamic integrations in molecular dynamics simulations using a noniterative method to include electronic polarization", *Chem. Phys. Lett.* **167**, 252 (1990).